Fault-tolerant quantum repeaters with minimal physical resources, and implementations based on single photon emitters

L. Childress,[1] J. M. Taylor,[1] A. S. Sørensen,[1,2,3] and M. D. Lukin[1,2]

[1] *Department of Physics, Harvard University, Cambridge,Massachusetts, 02138*
[2] *ITAMP, Harvard-Smithsonian Center for Astrophysics, Cambridge,Massachusetts, 02138*
[3] *The Niels Bohr Institute, University of Copenhagen, DK-2100 Copenhagen Ø, Denmark*

(Dated: February 9, 2008)

We analyze a novel method that uses fixed, minimal physical resources to achieve generation and nested purification of quantum entanglement for quantum communication over arbitrarily long distances, and discuss its implementation using realistic photon emitters and photonic channels. In this method, we use single photon emitters with two internal degrees of freedom formed by an electron spin and a nuclear spin to build intermediate nodes in a quantum channel. State-selective fluorescence is used for probabilistic entanglement generation between electron spins in adjacent nodes. We analyze in detail several approaches which are applicable to realistic, homogeneously broadened single photon emitters. Furthermore, the coupled electron and nuclear spins can be used to efficiently implement entanglement swapping and purification. We show that these techniques can be combined to generate high-fidelity entanglement over arbitrarily long distances. We present a specific protocol that functions in polynomial time and tolerates percent-level errors in entanglement fidelity and local operations. The scheme has the lowest requirements on physical resources of any current scheme for fully fault-tolerant quantum repeaters.

PACS numbers: 03.67.Hk, 03.67.Mn, 78.67.Hc

I. INTRODUCTION

Quantum communication holds promise for transmitting secure messages via quantum cryptography, and for distributing quantum information [1]. However, exponential attenuation in optical fibers fundamentally limits the range of direct quantum communication techniques [2], and extending them to long distances remains a conceptual and technological challenge.

In principle, the limit set by photon losses can be overcome by introducing intermediate quantum nodes and utilizing a so-called quantum repeater protocol [3]. Such a repeater creates quantum entanglement over long distances by building a backbone of entangled pairs between closely-spaced quantum nodes. Performing an entanglement swap at each intermediate node [4] leaves the outer two nodes entangled, and this long-distance entanglement can be used to teleport quantum information [5, 6] or transmit secret messages via quantum key distribution [7]. Even though quantum operations are subject to errors, by incorporating entanglement purification [8, 9] at each step, one can extend entanglement generation to arbitrary distances without loss of fidelity in a time that scales polynomially with distance [3]. This should be compared to direct communication, which scales exponentially, making it impractical for long distances.

Several approaches for physical implementation of a quantum repeater protocol have been proposed. Early work was based on systems of several atoms trapped in high finesse optical cavities [10, 11, 12]. Such systems can form a quantum network with several quantum bits (qubits) per node, and are particularly suitable for efficient implementation of the pioneering proposal of Ref. [3]. In this approach, quantum communication over thousand kilometer distances requires seven quantum bits per node, which must be coherently coupled to perform local quantum logic operations, i.e. a seven qubit quantum computer. The specific implementation of these early ideas involved the techniques of cavity QED for interfacing stationary and photonic qubits and for performing the necessary quantum logic operations [13, 14]. Recent related work pointed out that long-distance entanglement can be implemented via probabilistic techniques without the use of ultra-high finesse cavities [11, 12], while local operations can be accomplished via short-range interactions involving e.g. interacting trapped ions. However, few-qubit registers are still technically very difficult to construct, and the difficulty increases drastically with the number of qubits involved. At the same time, a novel approach based on photon storage in atomic ensembles [15] and probabilistic entanglement is also being actively explored. In comparison with systems based on many-qubit nodes, this approach offers less error tolerance and requires a longer communication time. Realization of a robust, practical system that can tolerate all expected errors remains therefore a challenging task.

In a recent paper [16] we proposed a quantum repeater protocol which could be implemented using the electronic and nuclear degrees of freedom in single photon emitters. Here we present further details of the proposal described in Ref. [16], and we compare our methods to alternative strategies. We show that our repeater protocol requires only two effective quantum bits at each node. This is the minimum requirement on physical resources which still allows active error correction. As a specific implementation, we consider nodes formed by a single quantum emitter with two internal degrees of freedom. A pair of electronic spin sublevels allows for state-selective optical

excitation (see inset in Figure 1a), and a proximal nuclear spin provides an auxiliary memory. State-selective fluorescence is used for probabilistic entanglement generation between electronic spin degrees of freedom. We analyze in detail and compare several approaches for probabilistic entanglement generation, focussing on the feasibility of their implementation using realistic photon emitters. Once electronic spin entanglement is generated, the coupled electron and nuclear spin at each node can be used to efficiently implement entanglement swapping and purification. We show that these techniques can be combined to generate high-fidelity entanglement over arbitrarily long distances. We present a specific protocol that functions in polynomial time and tolerates percent-level errors in entanglement fidelity and local operations.

Our approach is stimulated by recent experimental progress in single photon generation by means of single quantum emitters, including atoms and ions as well as impurities and nanostructures in solid state devices. Although our approach is relevant to atomic systems, such as single atoms trapped in a cavity [17] or single trapped ions [12], it is particularly suitable for implementation with solid-state emitters, for example impurity color centers [18, 19] and quantum dots [20, 21]. These devices offer many attractive features including optically accessible electronic and nuclear spin degrees of freedom, potential opto-electronic integrability, and fast operation.

The paper is organized as follows. First, we will discuss techniques for entanglement generation. For clarity, we will present our results in the context of nitrogen-vacancy (NV) centers in diamond, and discuss alternative implementations at the end. Realistic imperfections, such as homogeneous broadening and limited selection rules, motivate a novel entanglement generation scheme based on state-selective Rayleigh scattering and interferometry. We calculate the success probability and entanglement fidelity for this scheme as implemented in NV centers, and compare this scheme to alternative schemes based on Raman scattering or optical π pulses, with success conditioned on detection of one or two photons. Next, we will show how hyperfine coupling between the electron spin and proximal nuclei permits entanglement swapping and purification. Performing these operations in parallel and employing a nesting scheme, we calculate the fidelity obtained and the time required to generate it as a function of distance. In addition, we compare this scheme to pioneering proposals [3, 15] for fault-tolerant quantum repeaters. Finally, we quantitatively discuss the feasibility of implementing a quantum repeater using NV centers, and elucidate alternative material systems which satisfy the requirements of our technique.

II. ENTANGLEMENT GENERATION

The initial step in our scheme is entanglement generation between the electron spins of two emitters separated by a distance L_0. In principle, entanglement can be generated probabilistically by a variety of means, e.g., Raman scattering [13, 22, 23] or polarization-dependent fluorescence [12]. However, for our repeater protocol it is essential that the optical transition be independent of the nuclear spin state, and solid state emitters do not always allow Raman scattering or polarization-dependent fluorescence which fulfills this requirement. We therefore consider an entanglement mechanism based on state-selective elastic light scattering as shown in Figure 1. Elastic light scattering places few restrictions on selection rules, and permits nuclear-spin-independent fluorescence as we discuss below.

A. Properties of single color centers

Our entanglement generation scheme is applicable to a wide variety of physical systems, requiring only the simple level structure illustrated in Fig. 1a. For clarity, we will present it first using a concrete example: the nitrogen-vacancy (NV) center in diamond, which has the specific level structure shown in Fig. 2. This example illustrates many generic features common to other solid-state emitters.

NV centers represent a promising physical system because of their strong optical transition around 637 nm and optically accessible electron spin states. In particular, the ground state (A_1 symmetry class of the C_{3v} group) has three electronic spin-states which we label $|-1\rangle$, $|0\rangle$ and $|1\rangle$ according to their spin angular momentum along the symmetry axis of the crystal (M_s). Spin-orbit and spin-spin effects lead to a splitting of $|0\rangle$ from $|\pm 1\rangle$ by 2.88 GHz. Since we only require two electronic spin states, $|0\rangle$ and $|1\rangle$, we isolate these two states from the $|-1\rangle$ state by either adding a small magnetic field to shift the energy of the $|\pm 1\rangle$ state, or by using appropriately polarised ESR-pulses. As spin-orbit and spin-spin effects are substantially different for the optically excited state (E symmetry class), the strong transition from the $M_s = 0$ sublevel of the ground orbital state can be excited independently of the other M_s states. Although there is evidence for photo-bleaching at low temperatures, current models indicate that crossover into the dark metastable state occurs primarily from the $M_s = \pm 1$ excited states [24]. Furthermore, crossover into the trapping state is a detectable error. In the repeater protocol described below we perform a series of measurements on the electronic spin. During these measurements, the dark state will not produce any fluorescence, revealing the error. Shelving into the metastable state will thus influence the time (see Appendix) but not the fidelity associated with the repeater protocol. Consequently, we assume that we are only near resonance with a single state $|e\rangle$ which has $M_s = 0$, and neglect photo-bleaching effects.

The electron spin degree of freedom suffices to generate entanglement between adjacent NV centers. To propagate entanglement to longer distances, we will make use

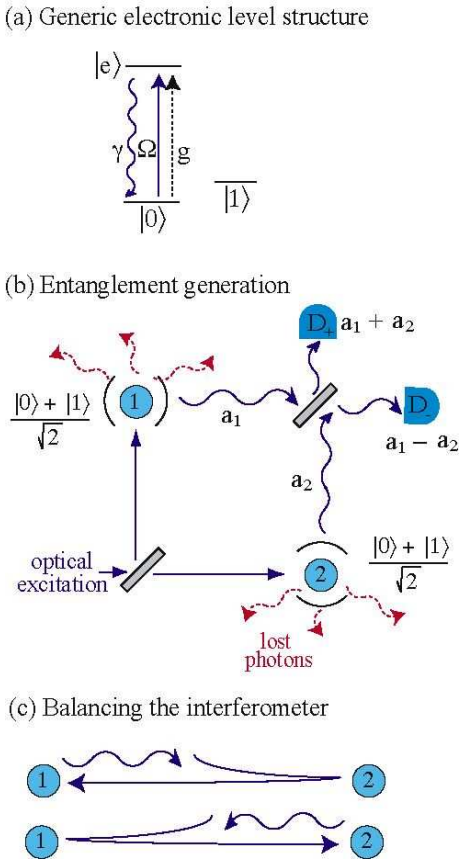

FIG. 1: *(a) Generic level structure showing the state-selective optical transitions and electronic spin sublevels required for entanglement generation. (b) Setup used to create entanglement. The two emitters act as state dependent mirrors in an interferometer. The outputs of the cavities (a_1 and a_2) are combined on a beamsplitter. By proper alignment of the interferometer the photons always exit through the $(a_1+a_2)/\sqrt{2}$ port if both centers are in the scattering state $|0\rangle$. A detection of a photon in the $(a_1-a_2)/\sqrt{2}$ mode thus leads to an entangled state. (c) Scheme for balancing the interferometer. Each node is optically excited by a laser pulse which first reflects off the other node, so that the optical path lengths for the two excitation/emission paths are identical.*

of an auxiliary nuclear degree of freedom $\{|\uparrow\rangle, |\downarrow\rangle\}$ which will be used for storage of quantum information during the repeater protocol. In NV centers, this nuclear degree of freedom can arise from a nearby carbon-13 impurity or directly from the nitrogen-14 atom that forms the center. The large energy separation between the $|0\rangle$ and $|\pm 1\rangle$ states exceeds the hyperfine interaction by an order of magnitude, decoupling the nuclear and electronic spins. The energy levels can thus be described by product states of the two degrees of freedom. Furthermore, in states with $M_s = 0$, the energy is independent of the nuclear state. Finally, a small magnetic field $\sim 10-100$ Gauss allows spectral resolution of the $M_s = \pm 1$ states without producing significant nuclear Zeeman splitting. The optical transition between $|0\rangle$ and $|e\rangle$ is thus disentangled from the nuclear spin state. Consequently, the nuclear spin can be used to store entanglement while the $|0\rangle - |e\rangle$ transition is used to generate another entangled pair of electron spins.

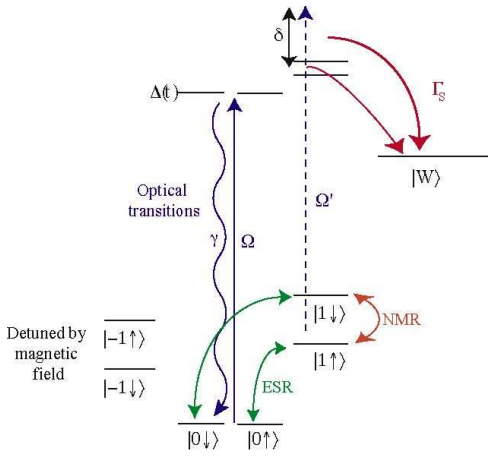

FIG. 2: *The relevant electronic and nuclear states of the coupled NV center and ^{13}C impurity nuclear spin. The electron spin states can be coupled by ESR microwave fields near 2.88 GHz, while the nuclear spin states can be addressed by NMR pulses on the 130 MHz hyperfine transition. A laser applied on resonance with the $M_s = 0$ optical transition produces strong fluorescence for the entanglement scheme; it will also weakly excite the $M_s = \pm 1$ transitions. In our model we assume that only the $M_s = \pm 1$ states decay to the shelving state $|W\rangle$ at rate Γ_S.*

B. Entanglement protocol

To implement the entanglement scheme, each NV center is placed inside a photonic cavity, whose output is coupled to a single-mode photonic fiber (note, however, that cavities are not essential for this proposal, see below). Fibers from adjacent NV centers enter two ports of a beamsplitter, and entangled electron spin pairs are obtained conditional on detection of a photon in an outgoing arm of the beamsplitter.

Specifically, our protocol for entanglement generation relies on scattering on the closed optical transition between $|0\rangle$ and $|e\rangle$. This scattering does not change the state of the NV center; the centers essentially act as mirrors reflecting the light only if they are in the state $|0\rangle$. We assume that each of the centers is initially prepared in the state $(|0\rangle + |1\rangle)/\sqrt{2}$, so that the total state is

$$|\Psi_{\rm ini}\rangle = \frac{1}{2}(|00\rangle + |11\rangle) + \frac{1}{2}(|01\rangle + |10\rangle). \qquad (1)$$

Since there is no light scattering from state $|1\rangle$, we can exclude the $|11\rangle$ component if we detect any scattered photons. In state $|00\rangle$, both centers act as mirrors, so that by balancing the interferometer in Fig. 1 (b) we can

arrange for the photons to leave through a specific port D_+ . A photon detection in the opposite port D_- can thus only arise from the $|01\rangle$ and $|10\rangle$ states and produces an entangled superposition of these two states.

Balancing and stabilizing an interferometer over tens of kilometers as required for the implementation of this protocol represents a considerable challenge. Using a method analogous to the plug-and-play system used in quantum key distribution [25], we can reduce this requirement to stabilization of a small interferometer locally at each detector. Suppose that we wish to generate entanglement between repeater nodes R_1 and R_2. Employing fast optical switches, we excite R_1 by sending a pulse of light toward R_2, where the light is reflected and sent past the detector to R_1. Light emitted from R_1 follows the same path back to the detector. Similarly, we excite R_2 by sending a pulse of light toward a fast switch at R_1. The two paths thus cover the same path length between the nodes and we are insensitive to fluctuations in the path lengths as long as these fluctuations happen on a time scale which is longer than the time it takes for the pulses to travel between the stations. Alternatively one could change to a protocol which relies on the detection of two photons instead of one. In such protocols the sensitivity to changes in the path lengths can be reduced considerably [26, 27, 28].

C. Entanglement fidelity in the presence of homogeneous broadening

We now describe this process mathematically, calculating the fidelity of the entangled pair produced by our protocol, as well as the probability for it to succeed. Our analysis incorporates dominant sources of error in solid-state systems; in particular, we account for effects of homogeneous broadening on the optical transition.

Our model assumes that the NV centers are excited by a weak driving field applied between the states $|0\rangle$ and $|e\rangle$ with Rabi frequency Ω; the excited states then radiatively decays at a rate γ. To describe the effect of homogeneous broadening on the optical transition we assume that the energy of the excited level fluctuates with a characteristic time which is slow compared to the optical frequency and much shorter than the lifetime of the excited state. In this approximation the broadening can be described by including a time-dependent detuning $\Delta(t)$ with white-noise characteristics: $\langle\Delta(t)\rangle = 0, \langle\Delta(t)\Delta(t')\rangle = \Gamma\delta(t-t')$. Below we shall be working in the limit of weak driving $\Omega \ll \gamma + \Gamma$. In this limit the light emitted from a center consists of two contributions: (i) a coherent part centered around the frequency of the driving laser with a width given by the width of the driving laser, and (ii) an incoherent part centered around the frequency of the transition with a frequency width of $\gamma + \Gamma$. The relative weight of these two contributions is $\gamma : \Gamma$. With considerable broadening of the optical transition $\Gamma \gtrsim \gamma$ it is therefore essential to filter out the incoherent scattered light with a frequency filter to get a high fidelity. To filter out the incoherent light and obtain a high collection efficiency we assume that the centers interact with an optical cavity with a coupling constant g and a decay rate κ. We emphasize, however, that good cavities are not essential for our proposal: we only require sufficient collection efficiency and frequency selectivity, which could also be obtained by collecting the light with a lens and sending it through a narrow frequency filter. In general the weak drive may be detuned from the excited state, which would simplify the filtering of coherent from incoherent light. However, off-resonant excitation would require a stronger driving field, making it harder to avoid stray light reaching the detectors. For simplicity we only discuss the situation where, on average, the driving field and cavity mode are resonant with the center.

The combined NV-center cavity system is then described by the Hamiltonian

$$H = \Delta(t)|e\rangle\langle e| + \frac{\Omega}{2}(|0\rangle\langle e| + |e\rangle\langle 0|) + g\hat{c}^\dagger|0\rangle\langle e| + g|e\rangle\langle 0|\hat{c}, \tag{2}$$

where $\hat{c}$ is the photon annihilation operator for the field in the cavity. In the Heisenberg picture, decay terms can be included by considering the quantum Langevin equations of motion for the atomic operators $\hat{\sigma}_{ij} = |i\rangle\langle j|$,

$$\frac{d\hat{c}}{dt} = -\frac{\kappa}{2}\hat{c} - ig\hat{\sigma}_{0e} + \hat{F}_c \tag{3}$$

$$\frac{d\hat{\sigma}_{0e}}{dt} = \left(-\frac{\gamma}{2} - i\Delta(t)\right)\hat{\sigma}_{0e} + i\left(g\hat{c} + \frac{\Omega}{2}\right)(\hat{\sigma}_{ee} - \hat{\sigma}_{00}) + \hat{F}_{0e} \tag{4}$$

$$\frac{d\hat{\sigma}_{ee}}{dt} = -\gamma\hat{\sigma}_{ee} + \left(i(\frac{\Omega}{2} + g\hat{c}^\dagger)\hat{\sigma}_{0e} + \text{h.c.}\right) + \hat{F}_{ee} \tag{5}$$

where the noise $\hat{F}_c$ is the incoming vacuum noise leading to cavity decay at rate κ and the other noise operators $\hat{F}_{0e}, \hat{F}_{ee}$ represent the effect of other optical modes that lead to decay.

We obtain an appropriate solution to the quantum Langevin equations by noting that, in the limit of weak driving, $\Omega \ll \gamma$, there is virtually no population of the excited state, $\hat{\sigma}_{00} - \hat{\sigma}_{ee} \approx \hat{\sigma}_{00}$. The solution can then be written in the form $\hat{c} = \alpha\hat{\sigma}_{00}$+noise and $\hat{\sigma}_{0e} = \beta\hat{\sigma}_{00}$+noise, but the equations for α and β are complicated due to the noise $\Delta(t)$. By averaging the Langevin equations over the noise one can, however, find simple equations for various moments of α and β, and by taking steady state solutions of the averaged equations we find

$$\overline{\alpha} = \frac{-2g\Omega}{\kappa(\gamma+\Gamma)(1+4g^2/\kappa(\gamma+\Gamma))} \tag{6}$$

$$\overline{|\alpha|^2} = \frac{\frac{4g^2\Omega^2}{\kappa^2(\gamma+\Gamma)^2}}{\left(1+\frac{4g^2}{\kappa(\gamma+\Gamma)}\right)\left(1-\frac{\Gamma\kappa}{(\gamma+\Gamma)(\gamma+\kappa)}+\frac{4g^2}{\kappa(\gamma+\Gamma)}\right)} \tag{7}$$

$$\overline{\beta} = \frac{-i\Omega}{(\gamma+\Gamma)(1+4g^2/\kappa(\gamma+\Gamma))}. \tag{8}$$

Note that in the presence of homogeneous broadening $\Gamma \neq 0$, the moments do not factor, $\overline{|\alpha|^2} \neq |\overline{\alpha}|^2$, signifying incoherent scattering of light into the cavity.

We now apply the entanglement generation protocol, and use our mathematical model to predict the average density matrix components of the NV center electron spins. In our scheme, we combine the output of the two cavities on a beamsplitter and select the desired entangled state by conditioning on a click in detector D_-, described by the photon annihilation operator $\hat{d}_- = \sqrt{\zeta\kappa/2}(\hat{c}_1 - \hat{c}_2)$. Here, subscripts one and two refer to the two NV-centers we are trying to entangle, ζ is the total collection and detection efficiency for photons leaving the cavity, and we have omitted the contribution from vacuum noise operators. To describe the effect of the detection, we use the quantum jump formalism[29]. If the system starts out in state $|\Psi_{\rm init}\rangle$, the density matrix element $\rho_{i,j}$ at time t can be found by

$$\rho_{i,j}(t) = \langle\Psi_{\rm init}|\hat{d}_-(t)^\dagger|j\rangle\langle i|\hat{d}_-(t)|\Psi_{\rm init}\rangle\delta t/\delta P, \quad (9)$$

where the time argument t is included to emphasise the time dependent Heisenberg operators, and where δP is the probability to have a click during a time δt,

$$\delta P = \langle\Psi_{\rm init}|\hat{d}_-(t)^\dagger\hat{d}_-(t)|\Psi_{\rm init}\rangle\delta t. \quad (10)$$

Our entanglement generation scheme relies on interference to eliminate D_- detection events coming from the initial state $|00\rangle$. However, according to our formalism, if we start out in an initial state $|00\rangle$ the probability to have a click is given by

$$\begin{aligned}\delta P &= \delta t\langle 00|\overline{\hat{d}_-^\dagger\hat{d}_-}|00\rangle \\ &= \kappa\zeta\delta t\Big(\overline{|\alpha|^2} - |\overline{\alpha}|^2\Big),\end{aligned} \quad (11)$$

where we assume the noise is independent for the two centers. This expression vanishes only for coherent scattering of light into the cavity, i.e. $\overline{|\alpha|^2} = |\overline{\alpha}|^2$ or $\Gamma = 0$. In the presence of broadening, there is a finite probability that light will be detected from the $|00\rangle$ state. Similarly, $\Gamma > 0$ leads to a finite probability for incoherent scattering from $|01\rangle$ and $|10\rangle$. Homogeneous broadening thus reduces the fidelity ($F = \langle\Psi_{\rm ideal}|\rho|\Psi_{\rm ideal}\rangle$, (where $|\Psi_{\rm ideal}\rangle$ denotes the ideal entangled state) by

$$\begin{aligned}1 - F &= \frac{3}{2}\left(1 - \frac{|\overline{\alpha}|^2}{\overline{|\alpha|^2}}\right) \\ &= \frac{3}{2}\frac{\Gamma}{\gamma+\Gamma}\frac{\kappa}{\gamma+\kappa}\frac{1}{1+4g^2/\kappa(\gamma+\Gamma)}.\end{aligned} \quad (12)$$

Here we are interested in the limit where the fidelity is close to unity and we shall therefore assume $\overline{|\alpha|^2} \approx |\overline{\alpha}|^2$ in the calculation of other noise sources below.

D. Other errors

In addition to the error caused by homogeneous broadening, there is also a reduction in fidelity caused by multiple spontaneous emission events from the centers. This fidelity can conveniently be expressed in terms of the total emission probability

$$P_{em} = \frac{t_0\Omega^2}{(\gamma+\Gamma)[1+4g^2/\kappa(\gamma+\Gamma)]}, \quad (13)$$

where t_0 is the duration of the applied laser pulse. In the absence of homogeneous broadening, multiple excitations result in a fidelity

$$F = \frac{1}{2} + \frac{{\rm e}^{-P_{em}(1-\epsilon/2)}}{2} \quad (14)$$

and success probability

$$P = (1 - \exp(-\epsilon P_{em}/2))/2. \quad (15)$$

The total collection efficiency can be expressed as $\epsilon = \zeta P_{\rm cav}$ with the probability to emit into the cavity given by

$$P_{\rm cav} = \frac{4g^2/\kappa(\gamma+\Gamma)}{1+4g^2/\kappa(\gamma+\Gamma)}. \quad (16)$$

This treatment has neglected the possibility of distinguishing multiple photon detection events. If our detector can resolve photon number, we can use the information to improve our protocol. In particular, a detection in the mode described by $\hat{d}_+ = \sqrt{\zeta\kappa/2}(\hat{c}_1 + \hat{c}_2)$+noise has no effect on the component of Eq. (1) that we are interested in, since $d_+(|01\rangle + |10\rangle) \propto (|01\rangle + |10\rangle)$. Furthermore, a detection in this plus mode contains contributions from $|00\rangle$, so it yields no useful information. On the other hand, detection events in the mode described by $\hat{d}_-$ change the sign of the superposition state, since $\hat{d}_-(|01\rangle + |10\rangle) \propto (|01\rangle - |10\rangle)$, and $\hat{d}_-(|01\rangle - |10\rangle) \propto (|01\rangle + |10\rangle)$. Consequently, the optimal strategy is to change the phase of the entangled state when an even number of photons is detected. The resulting fidelity is

$$F = \frac{1}{2} + \frac{{\rm e}^{-P_{em}(1-\epsilon)}}{2}. \quad (17)$$

Finally, we must include the effect of two other sources of noise: dark counts and electron spin dephasing. In the limit of small success probability P the dark count introduces an incoherent admixture of the initial state and thus leads to a reduction in fidelity $P_{\rm dark}/P$ where $P_{\rm dark} = \gamma_{dc}t_0$ is the dark count probability. Electron spin dephasing makes the state decay towards a state with fidelity $1/2$ at a rate $2\gamma_e$, yielding a reduction in the fidelity of γ_e times the total time of the experiments. Typically, this total time will be dominated by the classical communication time between nodes, t_c.

Putting these considerations together, we find that the entanglement scheme succeeds with probability $P = (1/2)\left(1 - e^{-P_{\rm em}\epsilon/2}\right) \approx \epsilon P_{\rm em}/4$, producing the state $|\Psi_-\rangle$ in time $T_0 \approx (t_0 + t_c)/P$ with fidelity

$$\begin{aligned}F_0 &= \frac{1}{2}\left(1 + e^{-P_{\rm em}(1-\epsilon)}\right) - \gamma_e(t_0 + t_c) \\ &\quad -\gamma_{dc}\frac{t_0}{P} - \frac{3}{2}\frac{\Gamma}{\Gamma+\gamma}\frac{\kappa}{\kappa+\gamma}\frac{1}{1+4g^2/\kappa(\gamma+\Gamma)}\end{aligned} \quad (18)$$

For realistic emitters placed into a cavity with either a narrow linewidth $\kappa \ll \gamma$ or a large Purcell factor $4g^2/(\kappa(\gamma+\Gamma)) \gg 1$, the first two terms should dominate the error.

III. COMPARISON TO OTHER ENTANGLEMENT GENERATION SCHEMES

The entanglement generation scheme that we have presented so far is the scheme that we believe to be best suited to NV centers. For other systems, this may not be the case. In particular, the presented scheme has two primary drawbacks: (1) it relies on resonant scattering, making it difficult to filter fluorescence photons from the applied laser field; (2) to avoid loss of fidelity from incoherent scattering, one must detect only a narrow frequency interval in the scattered light. Other entanglement methods present different problems which may prove easier to resolve or other methods may be better suited for different physical systems. Consequently, we now briefly compare the resonant scattering scheme presented above to alternate techniques.

A. Raman transitions

One of the first schemes considered for probabilistic entanglement generation [13, 22, 23] used Raman transitions in three level atoms. In such schemes, an electron spin flip between non-degenerate ground states $|0\rangle$ and $|1\rangle$ is associated with absorption of a laser photon and emission of a frequency shifted Raman photon. After interfering the emission from two atoms, detection of a Raman photon projects the two-atom state onto a state sharing at least one flipped spin. To avoid the possibility that both atoms emitted a Raman photon, the emission probability must be quite small $P_{\rm em} \ll 1$. In this limit, a photon detection event in detector $D_\pm$ results in an entangled spin state $|\Psi_\pm\rangle$.

The Raman scheme can be implemented using either a weak drive between states $|1\rangle$ and $|e\rangle$ or with a short strong pulse which puts a small fraction of the population into $|e\rangle$. Since the latter is equivalent to the single detection π-pulse scheme discussed below, here we consider only weak driving. The system can now be treated using the quantum Langevin-quantum jump approach formulated above. As before, homogeneous broadening on the optical transition leads to an incoherent contribution to the Raman scattered light, which reduces the entanglement fidelity in a manner similar to Eq. (12). Again, for optimal fidelity the coherent part should be isolated with a narrow frequency filter. If we assume perfect filtering and a small collection efficiency $\epsilon \ll 1$ the fidelity conditioned on a click is given by

$$F = 1 - P_{\rm em} \tag{19}$$

with success probability $P = P_{\rm em}\epsilon$.

In the limit of large fidelity $F \approx 1$, the Raman scheme has a success probability which is a factor of 4 higher than for our interferometric scheme. Furthermore, the Raman scheme has the advantage that stray light may be spectrally filtered from the Raman photons. Nevertheless, because of the hyperfine interaction in state $|1\rangle$, the transition frequency from $|1\rangle$ to $|0\rangle$ depends on the nuclear spin state. The associated detrimental effect on the nuclear coherence could potentially be avoided by using simultaneous transitions from $|1\rangle|\uparrow\rangle$ and $|-1\rangle|\downarrow\rangle$, which are degenerate. To our knowledge, however, fluorescence between $|e\rangle$ and $|1\rangle$ has not be observed, making it uncertain whether the Raman scheme can be implemented for the NV-centers [49].

B. π pulses

Time-gated detection offers an alternate method for distinguishing scattered photons from stray incident light. If an atom or NV center is excited by a sufficiently short, strong laser pulse, its population is coherently driven into the excited state. The excited state $|e\rangle$ then decays on a time scale $1/\gamma$. When the decay time is much longer than the incident pulse length, the excitation light and the photon emitted from the atom are separated in time, and can thus be distinguished. Entanglement is then generated conditional on the detection of one or two photons, as elucidated below.

1. Single detection

One particularly simple method for generating entanglement using π-pulses begins with each atom in a state

$$\cos(\phi)|1\rangle + \sin(\phi)|0\rangle. \tag{20}$$

The incident π-pulse excites the optically active state $|0\rangle$ to $|e\rangle$ with unit probability, and the spontaneously emitted photons are interfered on a beamsplitter and subsequently measured (as for the Raman scheme above). Provided $\phi \ll 1$ we can ignore the possibility that both atoms are in state $|0\rangle$. A photon detection in $D_\pm$ excludes the state $|11\rangle$, preparing the system in $|\Psi_\pm\rangle$.

As with other entanglement schemes, high-fidelity entanglement generation requires filtering the incoherent scattering caused by homogeneous broadening of the optical transition. In previous sections, we have proposed to use a frequency filter to separate the narrow peak (in frequency) of coherent scattered light from the broad incoherent background. In the present case, filtering can be done in the time domain. In the excitation process a coherence is established between $|1\rangle$ and $|e\rangle$, and following the excitation this coherence (the off-diagonal density matrix element) decays at a rate $\Gamma/2$. By only conditioning on photons emitted a very short time after the

excitation, during which the coherence has not had time to decay, a high quality entangled pair is produced.

To describe this process mathematically, we again assume that the atom is placed inside an optical cavity. In contrast to our previous calculations, we assume that the cavity has a broad linewidth to ensure that generated photons leave the system as fast as possible. In the limit $\kappa \gg g$, γ, and Γ we can adiabatically eliminate the cavity by setting $d\hat{c}/dt = 0$ in Eq. (3) so that if we omit the noise we obtain

$$\hat{c}(t) = \frac{2ig}{\kappa}\hat{\sigma}_{0e}. \tag{21}$$

Inserting this expression into Eqs. (4) and (4) we find

$$\overline{\hat{\sigma}_{0e}}(t) = \hat{\sigma}_{0e}(t=0)\exp\left(-\frac{\gamma_{\rm eff}+\Gamma}{2}t\right) \tag{22}$$

$$\overline{\hat{\sigma}_{ee}}(t) = \hat{\sigma}_{ee}(t=0)\exp\left(-\gamma_{\rm eff}t\right), \tag{23}$$

where the effective decay rate $\gamma_{\rm eff}$ is the decay rate enhanced by the Purcell effect

$$\gamma_{\rm eff} = \gamma\left(1+\frac{4g^2}{\kappa\gamma}\right). \tag{24}$$

To find the fidelity of the entangled state created with this method we again use Eqs. (9) and (10). For simplicity we only work in the limit of small collection efficiency $\epsilon \ll 1$. Conditioned on a click at time t after the excitation, the fidelity of the entangled state is

$$F = \cos^2(\phi)\left(\frac{1}{2}+\frac{1}{2}{\rm e}^{-\Gamma t}\right) \tag{25}$$

and the probability to have a click during the short time interval from t to $t+\delta t$ is

$$\delta P = 2\epsilon\gamma_{\rm eff}\delta t\sin^2(\phi){\rm e}^{-\gamma_{\rm eff}t}, \tag{26}$$

where the collection efficiency $\epsilon = \zeta P_{\rm cav}$ is again given by the collection efficiency for the light leaving the cavity ζ, and the probability to emit into the cavity is now given by

$$P_{\rm cav} = \frac{4g^2/\kappa\gamma}{1+4g^2/\kappa\gamma}. \tag{27}$$

The success probability for a given fidelity now depends on the ratio between the broadening and the effective decay rate $\Gamma/\gamma_{\rm eff}$. For $\Gamma = 0$, the procedure of initially transferring population from $|1\rangle$ to $|0\rangle$ and then applying a π-pulse between $|0\rangle$ and $|e\rangle$ is equivalent to a Raman transition, and Eqs. (25,26) indeed reproduces the same relation between success probability and fidelity given in Eq. (19). In the limit of small broadening, $\Gamma \ll \gamma_{\rm eff}$, the π-pulse scheme is advantageous over the interferometric scheme presented first. In particular, for a fixed fidelity $F \approx 1$ the success probability is a factor of 4 higher.

In the presence of broadening, however, the situation is different. To obtain a high fidelity we should detect only photons emitted within a short time T following the excitation. The average fidelity will then depend on two parameters ϕ and T. By optimizing these two parameters we find that for $F \approx 1$ the fidelity is

$$F = 1 - \sqrt{\frac{\Gamma}{8\gamma_{\rm eff}}}\sqrt{\frac{P}{\epsilon}}. \tag{28}$$

Since previous expressions (14) and (19) for $1-F$ depended linearly on P, this represents a much faster decrease in the fidelity. The $\pi-$pulse scheme is thus less attractive for homogeneously broadened emitters.

2. *Double detection*

If the collection efficiency is very high, it may be an advantage to rely on the detection of two photons instead of one [26, 27, 30, 31]. In this scheme, both atoms are initially prepared in $(|0\rangle+|1\rangle)/\sqrt{2}$ and a π-pulse is applied between $|0\rangle$ and $|e\rangle$. Following a detection in $D_\pm$ the populations in states $|0\rangle$ and $|1\rangle$ are interchanged and another π-pulse is applied between $|0\rangle$ and $|e\rangle$. Conditioned on clicks following both π pulses we can exclude the possibility that the atoms were initially in the same state and we are left with $|\Psi_\pm\rangle$ conditioned on appropriate detector clicks. In the absence of homogeneous broadening, this protocol produces an entangled state with fidelity F=1 with probability $P = \epsilon^2/2$. The double-detection scheme thus avoids the multiple photon emission errors inherent in the single-detection schemes.

With broadening of the optical transition, this is no longer the case. For $F \approx 1$, the relation between fidelity and success probability is now given by

$$F = 1 - \frac{\Gamma}{\gamma_{\rm eff}\epsilon}\sqrt{2P}. \tag{29}$$

Again the fidelity decreases more rapidly with the success probability than for the Raman and resonant scattering scheme, making it less useful for our purpose.

C. Summary

The best choice of scheme depends on the specific physical situation. The two π-pulse schemes are advantageous if the broadening is negligible. In particular, in the limit where we can ignore all errors except the photon attenuation, the double detection scheme results in the highest fidelity entangled pair. With low collection efficiency or large distances between emitters, the double detection will have a very small success probability because of the ϵ^2 factor, and it may be advantageous to rely on a single detection scheme.

The π-pulse schemes are less attractive if we are limited by homogeneous broadening of the optical transition because the fidelity decreases rapidly with the success probability. Better results are obtained for the resonant scattering or Raman schemes. When possible, the Raman scheme offers the best solution. The frequency-shifted Raman scattering allows frequency filtering of the incoming light; in addition the success probability is four times higher than for the resonant scattering scheme. But, as mentioned above, it is not always possible to drive Raman transitions , and it may be hard to achieve Raman transition which are independent of the nuclear spin state. For this reason we believe that the resonant scattering scheme is most promising in the particular case of NV-centers.

Finally we wish to add that the calculations we have performed here assume a specific model for the broadening (short correlation time for the noise). With other broadening mechanisms, e.g. slowly varying noise, these considerations will be different.

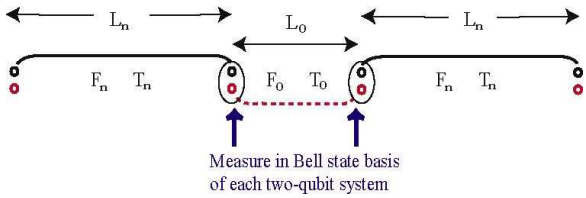

FIG. 3: *Entanglement propagation by swapping. To generate an entangled nuclear spin pair (black) over the distance $L_{n+1} = 2L_n + L_0$, we first generate nuclear entanglement over the first and second pair of repeater stations which are distance L_n apart. The electron spin (red) is then used to generate entanglement between the middle stations, separated by distance L_0. Nuclear (electron) spin entanglement is illustrated by solid (dashed) lines. Entanglement swapping is performed by measuring in the Bell state basis of the two-qubit system.*

IV. ENTANGLEMENT SWAPPING AND PURIFICATION

Using one of the procedures outlined above, electron spin entanglement can be generated between adjacent pairs of nodes. We now discuss a means to extend the entanglement to longer distances.

A. Swapping

After entangling nearest-neighbor electron spins, the electron spin state is mapped onto the auxiliary nuclear spin qubit for long-term storage using the hyperfine interaction. This operation leaves the electronic degree of freedom available to generate entanglement between unconnected nodes, as illustrated in Figure 3. By combining optical detection of individual electron spin states [32] and effective two-qubit operations associated with hyperfine coupling of electronic and nuclear spins [33], we may projectively measure all four Bell states in the electronic/nuclear manifold associated with each emitter. The outcomes of the Bell state measurements reveal the appropriate local rotations to obtain a singlet state in the remaining pair of nuclear spins, implementing a deterministic entanglement swap [4, 5]. By performing this procedure in parallel, and iterating the process for $N \propto \log_2(L/L_0)$ layers, we obtain the desired nuclear spin entanglement over distance L in a time $\propto L \log_2(L/L_0)$.

B. Purification

To extend entanglement to long distances in the presence of errors, active purification is required at each level of the repeater scheme. By performing local operations and measurements, it is possible to distill multiple entangled pairs with fidelity above some threshold F_{min} into a single entangled pair with higher purity[8, 9]. The purification algorithm we use is described in detail in Refs.[3, 9, 34, 35]. For clarity we will present it in a form appropriate to the system under consideration, which uses repeated generation of electron spin entangled pairs to purify a stored nuclear spin entangled pair. Specifically, an electron spin entangled pair between stations i and j is described by the density matrix diagonal components $\{a_e, b_e, c_e, d_e\}$ in the Bell state basis $\{|\Psi_-\rangle, |\Phi_+\rangle, |\Phi_-\rangle, |\Psi_+\rangle\}$, where

$$|\Psi_\pm\rangle_{ij}^{(e)} = \frac{1}{\sqrt{2}}\left(|0_i 1_j\rangle \pm |1_i 0_j\rangle\right) \quad (30)$$

$$|\Phi_\pm\rangle_{ij}^{(e)} = \frac{1}{\sqrt{2}}\left(|0_i 0_j\rangle \pm |1_i 1_j\rangle\right). \quad (31)$$

We will refer to these diagonal elements as the "vector fidelity" $\mathcal{F}_e = \{a_e, b_e, c_e, d_e\}$, noting that the first element $(\mathcal{F}_e)_1 = a_e$ encodes the fidelity with respect to the desired singlet state. A nuclear spin entangled pair between those stations is described by a similar vector fidelity $\mathcal{F}_n = \{a_n, b_n, c_n, d_n\}$ in the nuclear Bell basis

$$|\Psi_\pm\rangle_{ij}^{(n)} = \frac{1}{\sqrt{2}}\left(|\downarrow_i\uparrow_j\rangle \pm |\uparrow_i\downarrow_j\rangle\right) \quad (32)$$

$$|\Phi_\pm\rangle_{ij}^{(n)} = \frac{1}{\sqrt{2}}\left(|\downarrow_i\downarrow_j\rangle \pm |\uparrow_i\uparrow_j\rangle\right). \quad (33)$$

The purification protocol calls for a local rotation of each spin system at both locations:

$$|0\rangle_{i,j} \rightarrow \frac{1}{\sqrt{2}}\left(|0\rangle_{i,j} + i\,|1\rangle_{i,j}\right) \tag{34}$$

$$|1\rangle_{i,j} \rightarrow \frac{1}{\sqrt{2}}\left(|1\rangle_{i,j} + i\,|0\rangle_{i,j}\right) \tag{35}$$

$$|\downarrow\rangle_{i,j} \rightarrow \frac{1}{\sqrt{2}}\left(|\downarrow\rangle_{i,j} + i\,|\uparrow\rangle_{i,j}\right) \tag{36}$$

$$|\uparrow\rangle_{i,j} \rightarrow \frac{1}{\sqrt{2}}\left(|\uparrow\rangle_{i,j} + i\,|\downarrow\rangle_{i,j}\right), \tag{37}$$

followed by a two-qubit gate at each location:

$$\begin{array}{lll} |\downarrow 0\rangle_i \rightarrow |\downarrow 0\rangle_i & & |\downarrow 0\rangle_j \rightarrow |\downarrow 1\rangle_j \\ |\downarrow 1\rangle_i \rightarrow |\downarrow 1\rangle_i & & |\downarrow 1\rangle_j \rightarrow |\downarrow 0\rangle_j \\ |\uparrow 0\rangle_i \rightarrow -|\uparrow 1\rangle_i & & |\uparrow 0\rangle_j \rightarrow |\uparrow 0\rangle_j \\ |\uparrow 1\rangle_i \rightarrow -|\uparrow 0\rangle_i & & |\uparrow 1\rangle_j \rightarrow |\uparrow 1\rangle_j . \end{array} \tag{38}$$

After these operations, the electron spin is projectively measured at both locations. When the two electron spins are in the opposite state, the purification step succeeds, mapping the remaining nuclear spins to a diagonal state $\{a'_n, b'_n, c'_n, d'_n\}$ with $a'_n > a_n$.

This purification protocol can correct any type of error, but it functions best for phase errors, which correspond to diagonal elements of the form $\{f, 0, 0, 1-f\}$. To quantify the type of error associated with our entanglement generation scheme, we define a shape parameter υ such that the vector fidelity for entangled spin pairs between adjacent nodes is

$$\mathcal{F}_0 = \{F_0, (1-F_0)\upsilon, (1-F_0)\upsilon, (1-F_0)(1-2\upsilon)\}. \tag{39}$$

Note that $\upsilon \rightarrow 0$ corresponds to phase errors while $\upsilon \rightarrow 1/3$ corresponds to a Werner state with equal distribution of all error types. Note also that the assumption of diagonality imposes no restriction on the entangled states we generate, as any off-diagonal elements in their density matrices can be eliminated by performing random rotations (similar to the procedure for creating Werner states but without the symmetrization step)[35]. Furthermore, even without a randomization step, the average fidelity is determined by the diagonal elements [9].

C. Errors

In the presence of local errors in measurements and operations, the purification and swap procedures deviate from their ideal effect. To describe this we use the error model described in [34]. Measurement errors are quantified using a parameter η such that measurement projects the system into the desired state with probability η and into the incorrect state with probability $1-\eta$. For example, a projective measurement of state $|0\rangle$ would be

$$P_0 = \eta\,|0\rangle\langle 0| + (1-\eta)\,|1\rangle\langle 1|\,. \tag{40}$$

Errors in local operations are accounted for in a similar manner. With some probability p, the correct operation is performed; otherwise one traces over the relevant degrees of freedom in the density matrix and multiplies by the identity matrix (for further details see[34] and references therein). For example, the action of a two qubit operation U_{ij} would become

$$U_{ij}\rho U_{ij}^\dagger \rightarrow p\; U_{ij}\rho U_{ij}^\dagger + \frac{1-p}{4} Tr_{ij}(\rho)\otimes \mathcal{I}_{ij} \tag{41}$$

In our calculations, we neglect errors in single qubit operations and focus on two-qubit errors, which are likely to yield the dominant contribution.

These errors determine the level of purification which is possible given infinitely many purification steps. They also determine how much the fidelity degrades during the entanglement swap procedure. Below we describe a repeater protocol which, compared to the original proposal [3], reduces the required number of qubits at each repeater station at the expense of extra connection steps. Owing to these extra connection steps, our protocol is slightly more sensitive to local errors than the original scheme.

D. Nesting Scheme

Previous proposals for fault tolerant long distance quantum communication have required larger and larger numbers of qubits at each node as the communication distance is increased. Here we describe a nesting scheme which can be used to communicate over arbitrarily long distances while maintaining a constant requirement of only two qubits per node.

The scheme for nested entanglement purification is illustrated in Figure 4. For clarity, we will label purified pairs by"A", pairs to be purified by "B", and auxiliary pairs used to perform purification by "C". Briefly, an entangled pair ("B") is stored in the nuclear spins while an auxiliary entangled pair ("C") is generated in the electron spins. The purification protocol described in [9, 34] is then performed by entangling the electron and nuclear spins via the hyperfine interaction, and subsequently measuring the electron spins. Comparison of the measurement outcomes reveals whether the purification step was successful, resulting in a new stored pair B with higher fidelity. After successfully repeating the procedure for m purification steps, (a technique sometimes referred to as "entanglement pumping"), the stored pair becomes a purified ("A") pair, which can then be used to create B and C pairs over longer distances. We may thus generate and purify entanglement to arbitrary distances. This procedure is analogous to the scheme in Ref. [3], but avoids the increase in the number of qubits required for that proposal.

Mathematically, the scheme can be explained most easily using inductive arguments. Suppose that we have a means to create and purify entanglement over $k =$

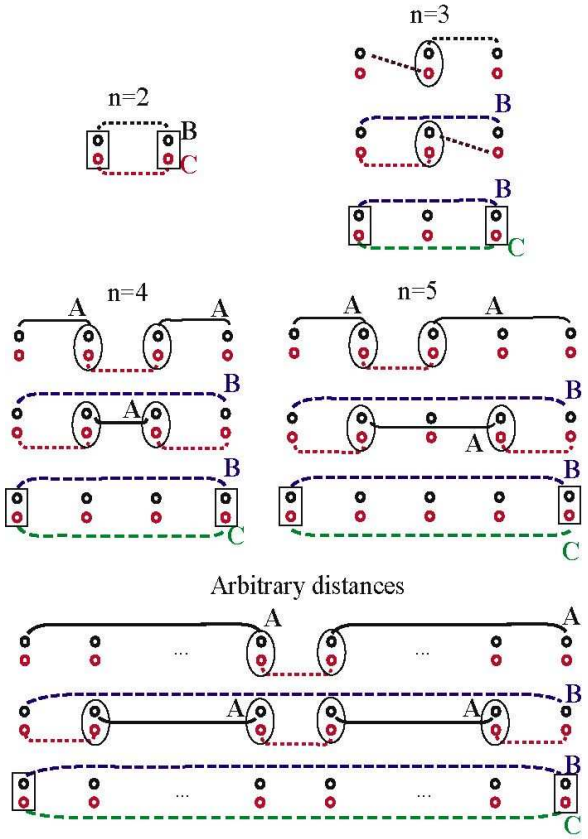

FIG. 4: *Nesting scheme for generation and purification of entangled nuclear and electron spin pairs. In each node, the nuclear spin degree of freedom is represented by the upper (black) circle, while the electron degree of freedom is represented by the lower (red) circle. Entanglement between different nodes is represented by a line connecting them. Ovals represent entanglement swap steps, and rectangles represent entanglement purification steps. For $n = 2$ the B and C pairs may be directly generated. For $n \geq 3$, the first step illustrates how the B pair is generated, while the remaining two steps illustrate how the C pair is generated while storing the B pair. The arbitrary distance algorithm works for $n \geq 6$.*

$2, 3, \cdots, n/2$ repeater stations ($(n+1)/2$ if n is odd), and that we know the vector fidelity $\mathcal{F}_A(k)$ and the time $\mathcal{T}_A(k)$ required for each distance. We can then determine the time required and the vector fidelity possible after purification over n repeater stations.

We begin by creating two purified nuclear spin A pairs over half the distance and connecting them via a central electron spin pair of vector fidelity $\mathcal{F}_0$. In the presence of local errors, this yields a nuclear spin B pair with vector fidelity

$$\mathcal{F}_B(n) = \mathcal{C}\left(\{\mathcal{F}_A(\frac{n}{2}), \mathcal{F}_0, \mathcal{F}_A(\frac{n'}{2})\}, \eta, p\right). \quad (42)$$

Here, $\mathcal{C}$ gives the vector fidelity obtained upon connecting the entangled pairs in the presence of local errors[35], and $n/2$ and $n'/2$ are understood to represent $(n-1)/2$ and $(n+1)/2$ when n is odd. The B pair is created in a time

$$\mathcal{T}_B(n) = \mathcal{T}_A(\frac{n'}{2}) + T_0 + \frac{n'}{2}t_c, \quad (43)$$

where T_0 is the time required to generate nearest-neighbour entanglement and t_c is the classical communication time between adjacent stations. We neglect the time required for local operations and measurement since these times are short compared to T_0 and nt_c. Similarly, we can find the vector fidelity and time for the electron spin C pair

$$\begin{aligned} \mathcal{F}_C(n) &= \mathcal{C}(\{\mathcal{F}_0, \mathcal{F}_A(\frac{n}{2}-1), \mathcal{F}_0, \mathcal{F}_A(\frac{n'}{2}-1), \mathcal{F}_0\}, \eta, p) \\ \mathcal{T}_C(n) &= \mathcal{T}_A(\frac{n'}{2}-1) + T_0 + (n-2)t_c. \end{aligned} \quad (44)$$

After performing one purification step, we obtain a nuclear spin pair A_1, with vector fidelity determined by the purification function $\mathcal{P}$

$$\mathcal{F}_{A_1}(n) = \mathcal{P}(\mathcal{F}_B(n), \mathcal{F}_C(n), \eta, p). \quad (45)$$

On average, the time required to perform this single step is

$$\mathcal{T}_{A_1}(n) = \frac{(\mathcal{T}_B(n) + \mathcal{T}_C(n) + (n-1)t_c)}{P_S(\mathcal{F}_B(n), \mathcal{F}_C(n))}, \quad (46)$$

where P_S is the probability that the purification step succeeds.

After m successful purification steps, the vector fidelity of the nuclear spin A_m pair is

$$\mathcal{F}_{A_m}(n) = \mathcal{P}(\mathcal{F}_{A_{m-1}}(n), \mathcal{F}_C(n), \eta, p), \quad (47)$$

and the average time required for its creation is

$$\begin{aligned} \mathcal{T}_{A_m}(n) &= \frac{\left(\mathcal{T}_{A_{m-1}}(n) + \mathcal{T}_C(n) + (n-1)t_c\right)}{P_S(m)} \quad (48) \\ &= (\mathcal{T}_C(n) + (n-1)t_c)\sum_{n=1}^{m}\prod_{k=n}^{m}\left(\frac{1}{P_S(m)}\right) \\ &\quad + \mathcal{T}_B(n)\prod_{k=1}^{m}\left(\frac{1}{P_S(m)}\right), \quad (49) \end{aligned}$$

where $P_S(m) = P_S(\mathcal{F}_{A_{m-1}}(n), \mathcal{F}_C(n))$. If we stop purifying at some fixed number M of purification steps, then the desired vector fidelity and time over distance n are given by

$$\begin{aligned} \mathcal{F}_A(n) &= \mathcal{F}_{A_M}(n) \quad (50) \\ \mathcal{T}_A(n) &= \mathcal{T}_{A_M}(n). \quad (51) \end{aligned}$$

To complete the inductive argument, we must show that the protocol works for small distances. There are many schemes one can use to generate and purify entanglement over shorter distances, and one possibility is illustrated in Figure 4. In fact, once the physical parameters for an implementation are determined, it should be possible to optimise the few-node scheme to minimise the required time or maximise the resulting fidelity.

E. Fixed point analysis

As the number of purification steps increases $m \to \infty$, the fidelity of the resulting entangled pair saturates. This saturation value can be found using a fixed point analysis (as described in[34]) by solving for the vector fidelity $\mathcal{F}_A$ which is unchanged by further purification steps

$$\mathcal{F}_A = \mathcal{P}\left(\mathcal{F}_A, \mathcal{F}_C, \eta, p\right), \tag{52}$$

where we have explicitly included the local errors in the purification function $\mathcal{P}$. This yields a fixed point fidelity $\mathcal{F}_{FP}(\mathcal{F}_C, \eta, p)$ which is independent of $\mathcal{F}_A$. Since the vector fidelity $\mathcal{F}_{\mathcal{A}}$ has three independent parameters characterising the diagonal elements of the density matrix, one might miss the fixed point. However, as the number of purification steps increases our simulations do indeed approach the calculated fixed point. We therefore calculate the fixed point as a function of distance to find the upper bound on the fidelity which can be attained for given $\mathcal{F}_0, L/L_0, p$, and η.

F. Asymptotic Fidelity

As the distance increases $L \to \infty$, the fixed point fidelity can approach an asymptotic value F_∞. We can understand the existence of F_∞ and its value by examining the protocol as a function of nesting level. In particular, to generate entanglement over n repeater stations we operate at nesting level $i \sim \log_2 n$, where we obtain a purified pair

$$\mathcal{F}_A^{(i)} = \mathcal{F}_{FP}(\mathcal{F}_C^{(i)}, \eta, p), \tag{53}$$

where $\mathcal{F}_{FP}$ is the fixed point solution to Eq. (52), and $(\mathcal{F}_{FP})_1 = F_{FP}$ is the fixed point fidelity. We will then use this purified pair $\mathcal{F}_A^{(i)}$ to build up an auxiliary C pair on the next nesting level $i+1$. Since the fidelity over distance $n-1$ is greater than that over distance n, i.e. $(\mathcal{F}_A(n-1))_1 \gtrsim (\mathcal{F}_A(n))_1$, the auxiliary pair fidelity we obtain will be greater than or equal to the first component of

$$\mathcal{F}_C^{(i+1)} \sim C(\{\mathcal{F}_A^{(i)}, \mathcal{F}_A^{(i)}, \mathcal{F}_0, \mathcal{F}_0, \mathcal{F}_0\}, \eta, p), \tag{54}$$

where C is again the connection function. This auxiliary pair will then determine $\mathcal{F}_A^{(i+1)} = \mathcal{F}_{FP}(\mathcal{F}_C^{(i+1)}, \eta, p)$. When $\mathcal{F}_A^{(i+1)} = \mathcal{F}_A^{(i)}$, we have reached the asymptotic fidelity $F_\infty = (\mathcal{F}_A)_1$ (see Figure 5), which is given by the intersection of the purification curve Eq. (53) and the auxiliary pair creation curve Eq. (54).

As was the case for the fixed point analysis, we must account for all diagonal components of the density matrix in the Bell state basis (not just the fidelity a). Consequently the asymptotic fidelity represents an upper bound to which the system may converge in the manner indicated by our simulations. Finally, we should stress that our calculations have not incorporated loss due to the long but finite memory time in the nuclear spins. This loss increases with the total time required for repeater operation, and sets the upper limit on the distance over which our scheme could operate.

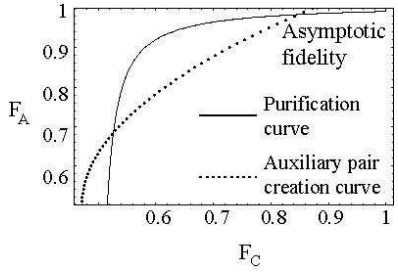

FIG. 5: *Approach to asymptotic fidelity. The solid curve shows the purified fidelity obtained from the auxiliary pair, while the dotted curve corresponds to the auxiliary pair (constructed from two smaller purified pairs) on the next nesting level. The system moves between the curves at each nesting step, and the upper intercept of the two curves gives the asymptotic fidelity. For this calculation* $F_0 = p = \eta = 0.99$, *and* $v = 0$.

G. Results

The discussion of final fidelity may be summarized as follows: the fidelity obtained at the end of this nested purification procedure, $F(m, L, F_0, p, \eta)$, depends on the number of purification steps m, the distance L between the outer nodes, the initial fidelity F_0 between adjacent nodes, and the reliability of measurements $\eta \leq 1$ and local two-qubit operations $p \leq 1$ required for entanglement purification and connection [34]. As the number of purification steps increases $m \to \infty$, the fidelity at a given distance L approaches a fixed point $F \to F_{FP}(L, F_0, p, \eta)$ at which additional purification steps yield no further benefit [34]. Finally, as L increases, the fidelity may approaches an asymptotic value $F_{FP} \to F_\infty(F_0, p, \eta)$. Figure 6a illustrates the efficiency of the purification protocol: for initial fidelities $F_0 \gtrsim 97\%$, three purification steps suffice to produce entanglement at large distances.

Figure 6b demonstrates that our scheme permits generation of high-fidelity, long distance entangled pairs in the presence of percent-level errors in polynomial time. Because solid-state devices allow fast operations and measurements, the overall time scale is set by the classical communication time between nodes. As an example, using a photon loss rate of ~ 0.2 dB/km and inter-node separation $L_0 \sim 20$ km (so that in the limit of good detectors the collection efficiency is $10^{-0.4} \sim 1/e$), a fidelity set by an emission probability $P_{\rm em} \sim 8\%$, local errors $\eta = p = 0.5\%$, and just one purification step at each nesting level, our scheme could potentially produce entangled pairs with fidelity $F \sim 0.8$ sufficient to violate Bell's inequalities over 1000 km in a few seconds. For

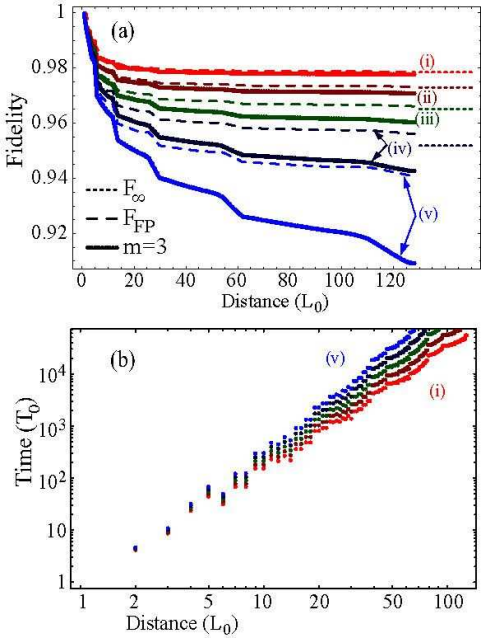

FIG. 6: *(a) Fidelity scaling with distance. Points show results using 3 purification steps at each nesting level; dashed lines show the fixed point F_{FP} at each distance; dotted lines indicate the asymptotic fidelity F_∞. For (a) and (b), measurements and local two-qubit operations $\eta = p$ contain 0.5% errors. The initial fidelity F_0 is (i) 100% (ii) 99% (iii) 98% (iv) 97% (v) 96% with phase errors only. (b) Average time scaling with distance for m=3, given in units of $T_0 = (t_0 + t_c)/P$, the time required to generate entanglement between nearest neighbors, and L_0, the distance between nearest neighbors. Measurement and local operation times are neglected. Note that the axes are logarithmic, so time scales polynomially with distance.*

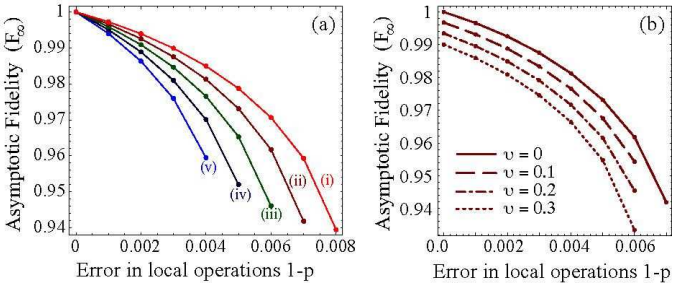

FIG. 7: *(a) Long-distance asymptote dependence on initial fidelity F_0 of (i) 100% (ii) 99% (iii) 98% (iv) 97% (v) 96% with phase errors only. (b) Long-distance asymptote dependence on error type. For the calculations shown, $F_0 = 0.99$, and the shape parameter ranges from $\upsilon = 0$ to $\upsilon = 0.3$. In both (a) and (b) measurement errors are set equal to operational errors, $\eta = p$.*

comparison, under the same set of assumptions direct entanglement schemes would require $\sim 10^{10}$ years.

Fig. 7a shows that our scheme will operate in the presence of $1-p \lesssim 1\%$ errors in local operations and percent-level phase errors in initial entanglement fidelity. Other types of error are in principle possible, and we consider nonzero shape parameters υ for the initial fidelity $\mathcal{F}_0$ in Eq. (39). The asymptotic fidelity shown in Fig. 7b indicates that, although the protocol we use is most effective for purifying phase errors, it also tolerates arbitrary errors.

H. Optimization

Once the parameters of the system are established, the protocol can be optimised to minimise the time required to generate some minimum fidelity F_{min} over a distance L. We can vary the number of repeater stations $\sim L/L_0$ and the number of purification steps m (which need not be constant). We can also tailor the entanglement generation procedure by changing the emission probability P_{em} to find the optimum balance between initial infidelity $1 - F_0 \sim P_{em}$ and entanglement generation time $T_0 \propto 1/P_{em}$. Finally, one could use more advanced optimal control techniques to vary the details of the protocol itself. In particular, it should be possible to speed up the algorithm by working simultaneously on multiple nesting levels, beginning entanglement generation and connection on the next nesting level as soon as the interior nodes are free. Further speed-up may also be possible in the case when collection efficiency is very high by using coincidence detection in combination with e.g. time-bin encoding [1]. As noted previously such coincidence detection could also be advantageous for interferometric stability [26, 27, 28].

Ultimately, the speed of this protocol is limited by three factors: classical communication time between nodes, probabilistic entanglement generation, and sequential purification. Faster techniques will require more efficient entanglement generation or larger numbers of qubits at each node to allow simultaneous purification steps.

I. Comparison to other quantum repeater schemes

This scheme combines the advantages of two pioneering proposals for quantum repeaters [3, 15]. Early work showed that entanglement purification and swapping could be combined to permit efficient, fault-tolerant quantum communication over distances longer than an attenuation length [3]. This scheme incorporated error correction at the cost of increased physical resources, requiring nodes containing a number of qubits scaling at minimum logarithmically with distance [34]. Owing to the difficulty of implementing even few-qubit quantum computation, implementation of this scheme remains a challenging goal. Our scheme is closely related to the original proposal with one key difference: by spatially rearranging the required physical resources, we can efficiently simulate their protocol while maintaining a con-

stant requirement on qubits per node. This makes our scheme amenable to realistic physical implementation.

Another physical implementation for quantum repeaters uses atomic ensembles as a long-lived memory for photons[15]. Entanglement is generated by interfering Raman scattered light from two ensembles. The entanglement is probabilistically swapped using an EIT readout technique. This scheme elegantly avoids effects of the dominant photon loss error by conditioning success on photon detection. Our scheme primarily differs from this proposal in two ways: first, access to two-qubit operations between electron and nuclear spin permits deterministic entanglement swapping; second, the two-qubit nodes allow active correction of arbitrary errors.

V. PHYSICAL SYSTEMS

We conclude with three specific examples for potential implementation of the presented method.

A. Implementation with NV centers

The NV center level structure illustrated in Fig. 2 allows implementation of all steps in the repeater protocol. The cycling transition from $|0\rangle$ to $|e\rangle$ is used for electron spin initialization by measurement, entanglement generation, and electron spin state measurement. A series of ESR and NMR pulses can be used to perform arbitrary gates between the electron spin and an adjacent ^{13}C spin [33]. Consequently, nuclear spin state initialization and measurement is achieved by initializing the electron spin, mapping the nuclear spin state onto the electron spin, and subsequently measuring the electron spin. Entanglement propagation and purification can be implemented in NV centers by driving ESR and NMR transitions and using optical detection of the electron spin states. Once electron spin entanglement is established between nodes R_i and R_{i-1}, it can be transferred to the nuclear spins, leaving the electron degree of freedom free to generate entanglement between station R_i and R_{i+1}. Provided that we can reinitialize the electron spin without affecting the nuclear entanglement, we can perform the same probabilistic entanglement procedure. Note that ESR multiplexing is required to perform a $\pi/2$ pulse independent of the nuclear spin; this can be accomplished simply by applying two ESR pulses at the two transition frequencies.

We now consider the feasibility of implementing our repeater protocol using NV centers in diamond. Owing to the overlap of electron wavefunctions in the ground and excited states, most of the NV center optical emission goes into the phonon sidebands. Other color centers in diamond, for example the NE8 center [36, 37] may suffer less from this drawback. To enhance the relative strength of the zero-phonon line, it will be necessary to couple the NV center to a cavity. For NV centers coupled to cavities with Purcell factors ~ 10 [21], we find that the dominant source of error is electron spin decoherence during the classical communication period. Using an emission probability $P_{\rm em} \sim 5\%$, a collection efficiency $\epsilon \sim 0.2$, and a classical communication time of $t_c \sim 70\mu$s over $L_0 \sim 20$ km, we find the fidelity of directly entangled pairs can reach $F_0 \sim 97\%$ for electron spin coherence times in the range of a few milliseconds. Electron spin coherence times in the range of 100μs have been observed at room temperature and significant improvements are expected for high purity samples at low temperatures [38]. The large hyperfine splitting allows fast local operations between electron and nuclear spin degrees of freedom on a timescale ~ 100ns [33] much shorter than the decoherence time, allowing $1-p < 1\%$. Finally, cavity enhanced collection should significantly improve observed measurement efficiencies of $\eta \sim 80\%$ [33].

B. Alternative implementation: quantum dots

Our discussion thus far has attempted to remain general while exemplifying our proposal using NV centers. The basic idea of using two-qubit repeater stations should be applicable to a wide variety of systems featuring coupled electron and nuclear spins. To illustrate an alternative implementation, we consider doped self-assembled quantum dots whose electron spin is coupled to collective nuclear states in the lattice. Compared to NV centers, this system offers large oscillator strengths and the potential for Raman manipulation. Doped semiconductor quantum dots have been considered in a variety of quantum computing proposals and related technologies [39, 40]. The spin state of the dopant electron provides a natural qubit with relatively long coherence times. Assuming a high degree of nuclear spin polarization ($P_{\rm n} \gtrsim 0.95$) [41] and active ESR pulse correction, the electron spin dephasing time is expected to be 1 ms [42]. The spins of lattice nuclei in the quantum dot provide an additional, quasi-bosonic degree of freedom with extremely long coherence times (~ 1 s with active correction [43]). Such ensembles of nuclear spin have been considered for use as a quantum memory [44] and, by taking advantage of the non-linearity of the Jaynes-Cummings Hamiltonian, as a fundamental qubit for a quantum computer [45].

Unlike the spin triplet state of the NV centers, the conduction band electron has two states, $|\uparrow\rangle$ and $|\downarrow\rangle$, corresponding to spin aligned and anti-aligned with an external magnetic field $B_{ext}||\hat{z}$. The quantum dot system also differs from NV centers in that it can be manipulated using Raman transitions: when the external field and growth direction are perpendicular (Voigt geometry), two allowed optical transitions to a trion state produce a lambda system ; moving towards aligned field and growth directions (Faraday geometry) suppresses the"forbidden" transitions, as shown in Fig. 8a.

Electron spin coherence can thus be prepared via Ra-

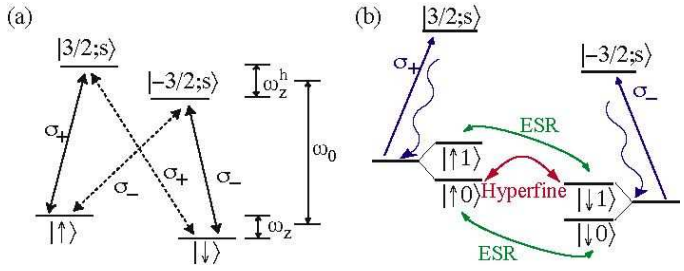

FIG. 8: *(a) Level structure for single electron to trion transition in a single-electron doped III-V or II-VI quantum dot with external magnetic field in close to a Faraday geometry with Zeeman splitting ω_z, heavy-hole splitting ω_z^h and up to four optical fields of different frequency and polarization. Dashed lines indicate weak dipole moments due to small magnetic field mixing. The triplet two-electron states are not included due to a large ($> 1meV$) exchange energy allowing for complete suppression of their effects. (b) Electronic ($|\uparrow\rangle, |\downarrow\rangle$) and collective nuclear ($|0\rangle, |1\rangle$) states and their transitions for singly doped quantum dots in a polarized nuclear spin lattice.*

man transitions or by standard ESR setups, and changes in effective magnetic field can be accomplished by off-resonant, spin-dependent AC Stark shifts with σ_+ light.

Although optical transitions in doped quantum dots can exhibit homogeneous broadening $\Gamma \sim 100$ GHz$\sim 10 - 100\gamma$ [46], the corresponding error can be made negligible by sending the output from the cavity through a frequency filter with a linewidth of a few hundred MHz. [50] Moreover, we note that InAs quantum dots have been successfully coupled to microcavities with Purcell factors ~ 10 [21].

Whereas the NV center electron spin was coupled to a single nuclear impurity, the electron in a quantum dot couples to collective excitations of many thousands of nuclei. We briefly discuss this system; further details are given in Refs. [44, 47]. The Hamiltonian governing this interaction is

$$H_{qd} = \omega_z \hat{S}_z + \hbar \sum_k \gamma_k \hat{I}_z^k + \hbar\Omega \sum_k \lambda_k \hat{\vec{S}} \cdot \hat{\vec{I}}^k, \qquad (55)$$

where γ_k is the gyromagnetic ratio for nuclear spin $\hat{\vec{I}}^k$, the nuclear spin coupling amplitudes satisfy $\lambda_k \propto |\psi(r_k)|^2$, $\sum_k \lambda_k^2 = 1$, and $\Omega = A/\hbar \sum_k \lambda_k$ (A is the hyperfine interaction constant). By identifying collective nuclear spin operators, $\hat{\vec{A}} = \sum_k \lambda_k \hat{\vec{I}}$, the hyperfine term may be written $\hbar\Omega \hat{\vec{S}} \cdot \hat{\vec{A}}$. For simplicity we restrict the following discussion to the case of perfect nuclear polarization (so the initial state of all N_n nuclear spins in the quantum dot is $|0\rangle = |-I\rangle \otimes \ldots \otimes |-I\rangle$ for I-spins). Then an effective Jaynes-Cummings type Hamiltonian describes the system:

$$H_{qd}^{eff} = \hbar\omega_z^{eff} \hat{S}_z + \hbar\Omega/2(\hat{A}_+ \hat{S}_- + \hat{A}_- \hat{S}_+). \qquad (56)$$

with corrections of order $\Omega/\sum_k \lambda_k \sim A/N_n$. The effective Zeeman splitting $\omega_z^{eff} = \omega_z - IA/\hbar$ is dominated by the field associated with the polarized nuclear spins ; for example, in GaAs quantum dots, this Overhauser shift is $IA/\hbar \sim 33$GHz. The large detuning ω_z^{eff} suppresses interactions which exchange energy between the electron and nuclear spins. By changing the effective magnetic field, we can shift the system into resonance $\omega_z^{eff} \to 0$ to drive Rabi oscillations between the electron spin and the collective nuclear state, see figure 8b. Pulsing the appropriate effective field permits a controllable map between the electron spin state and the collective nuclear degrees of freedom spanned by $|0\rangle$ and $|1\rangle = \hat{A}_+ |0\rangle$. In addition, more complicated sequences of electron-nuclear spin interaction and electron spin manipulation allow for arbitrary two qubit operations on $|\uparrow\rangle, |\downarrow\rangle$ and $|0\rangle, |1\rangle$ (see Ref. [45] and commentary therein).

Measurement and initialization proceed in much the same manner as described for NV centers. The state of the electron spin system can be read out by exciting a cycling transition with resonant σ_+ light, and measurement and ESR (or Raman transitions) can be employed to initialize the system in the desired state. As the effective Knight shift of the electron spin is negligible on the time scales of entanglement preparation, the collective nuclear state's coherence is unaffected by this process. Due to the improved selection rules and possibility of Raman transitions, it may be more effective to use the Raman entanglement generation scheme.

The nuclear state of the quantum dot can be prepared by cooling the nuclear spins using preparation of electron spin and manipulation of the effective magnetic field [48]. In practice, this leaves the nuclear system in a state $|\mathcal{D}\rangle$ with the same symmetry properties as the state $|0\rangle$ described above [47]. To date, 60% nuclear spin polarization has been achieved by optical pumping in GaAs quantum dots [41]. As was the case with NV centers, the nuclear spin state can be read out by preparing the electron spin in the $|\downarrow\rangle$ state, mapping the nuclear state to the electron spin state, and measuring the electron spin state.

C. Atomic Physics Implementation

Compared to the solid state implementations we have considered so far, implementations in single trapped atoms or ions have the advantage that they typically have very little broadening of the optical transitions. Because atomic systems do not reside in a complicated many-body environment, their internal degrees of freedom can have very long coherence times. For most atomic systems, however, it is hard to identify a mechanism which allows one degree of freedom, e.g., the nuclear spin, to be decoupled while we probe some other degree of freedom, e.g., the electron spin. Below we describe a system which does fulfill this requirement, although practical considerations indicate implementation may be challenging.

We consider alkali-earth atoms, such as neutral magnesium, and chose an isotope with non-vanishing nuclear

spin (^{25}Mg). The lowest lying states of magnesium are shown in Fig. 9 (electronic structure only). Instead of the electronic spin states we have considered so far, i.e., for NV centers and quantum dots, we will use states which differ both in spin and orbital angular momentum. The stable ground state $^1S_0$ will serve as state $|0\rangle$. In this state, the electronic degrees of freedom have neither spin nor orbital angular momentum and the nuclear spin is thus decoupled from the electronic state. The excited state $^3P_0^o$ (whose hyperfine interactions also vanish to leading order) will provide state $|1\rangle$. Note that the triplet-singlet transition from $^3P_0^o$ to the ground state is highly forbidden and this state has an extremely long lifetime, but transitions between the two states can still be induced with a strong laser.

To create entanglement we couple the ground state to the excited state $^1P_1$ with a laser field and collect the scattered light. From this excited state the atom essentially always decays back into the ground state. If the driving is detuned much further than the hyperfine splitting in the excited state, the nuclear spin is also decoupled during this process. The nuclear spin can therefore by used to store information while we entangle the electronic state with another atom. Finally, to implement gates between the electronic and nuclear states one should, for instance, couple the $|0\rangle$ state to another state in the atom where there is a hyperfine interaction, for example using resonant excitation of the $^1P_1$ state.

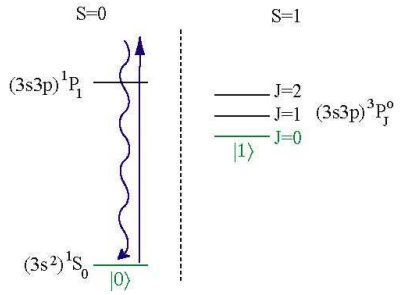

FIG. 9: *Electronic level structure of atomic magnesium. The electronic ground state $^1S_0$ has vanishing spin and orbital angular momentum. In this state the nuclear spin therefore decouples from the electronic degrees of freedom. An entangling operation which is also insensitive to the nuclear degree of freedom can be achieved with lasers which are detuned much further than the hyperfine splitting in the $^1P_1$ level.*

Finally, we note that all three physical implementations we suggest operate in the visible or near-IR, and will likely require high-efficiency frequency conversion to telecom wavelengths for low-loss photon transmission.

VI. CONCLUSION

In conclusion, we propose a method for fault tolerant quantum communication over long distances requiring only probabilistic nearest-neighbor entanglement generation, two-qubits per node, and two-qubit operations. We compare several schemes for entanglement generation and discuss two solid-state systems and an atomic system which might be used to implement them. Potential applications include secure transmission of secret messages over intercontinental distances.

The authors wish to thank Phillip Hemmer, Aryesh Mukherjee, Klaus Mølmer, Alexander Zibrov, and Gurudev Dutt. This work is supported by DARPA, NSF, ARO-MURI, and the Packard, Sloan and Hertz Foundations and the Danish Natural Science Research Council.

VII. APPENDIX

Photo-bleaching is a detectable error, so it does not affect the fidelity of entanglement generation or measurement, as we described above. However, it can increase the time required for these operations. Fluorescence correlation experiments are consistent with assigning a metastable singlet structure to the shelving state, which is coupled strongly to the $M_s = \pm 1$ excited states but only weakly to the $M_s = 0$ excited state (see Figure 2), [24]. We need to account for the possibility that our NV center bleaches during entanglement generation, requiring us to start over. During each attempt we resonantly excite the $M_s = 0$ transition with some probability $P_{\rm em}$ (see Eq. 13). To quantify the population lost to $|W\rangle$ we will consider a model where the $M_s = \pm 1$ excited states decay to the shelving state at rate Γ_S. The oscillator strength for the $M_s = \pm 1$ optical transitions are unknown, so we will assume that the Rabi frequencies on the $M_s = \pm 1$ transitions are Ω'.

During one attempt at entanglement generation, the probability to end up in the shelving state is

$$P_W \sim \Gamma_S \frac{\Omega'^2}{\delta^2} t_0, \tag{57}$$

where δ is the detuning from the $M_s = \pm 1$ optical transition. (The excited state energies are strongly inhomogeneously broadened, so δ is not precisely known; this detuning should be controllable using strain or applied electric fields.) On average, a large number of attempts $\sim 4/P_{\rm em}\epsilon^2$ are required for successful entanglement generation. Consequently the total probability for the system to end up in the shelving state during entanglement generation is

$$P_W \sim 4\Gamma_S \frac{\Omega'^2}{\delta^2}\frac{\gamma}{\Omega^2\epsilon^2} \sim 4\frac{\Gamma_S\gamma}{\delta^2\epsilon^2}\frac{\mu'^2}{\mu^2}, \tag{58}$$

where $\mu(\mu')$ is the oscillator strength for the $M_s = 0(\pm 1)$ transition. The precise values of these parameters are unknown, but we can estimate their order of magnitude: $\Gamma_S \sim 1 - 10$ MHz, $\gamma + \Gamma \sim 100$ MHz, $\delta \sim 1$ GHz, $\mu' \sim \mu$, yielding

$$P_W \sim \frac{4(10^{-3} - 10^{-4})}{\epsilon^2}. \tag{59}$$

If this error rate is too large, we can also check for photo-bleaching at intervals during the entanglement procedure.

The shelving state poses a similar problem during measurement. In this case, the $M_s = 0$ transition is strongly illuminated so that at least one photon reaches the detectors: $P_{\rm em} \sim 1/\epsilon^2$. Under the same illumination, any population in $|1\rangle$ will end up in the shelving state with probability

$$P_W \sim P_{\rm ex}\frac{\Gamma\gamma}{\delta^2}\frac{\mu'^2}{\mu^2} \sim \frac{\Gamma\gamma}{\delta^2\epsilon^2}\frac{\mu'^2}{\mu^2} \sim \frac{(10^{-3}-10^{-4})}{\epsilon^2}, \quad (60)$$

Note that the measurement fidelity is unaffected by photo-bleaching if we verify that the center is optically active by observing fluorescence either directly from the $|0\rangle$ state or after applying a multiplexed ESR pulse to the $|1\rangle$ states. Ultimately, in this model the only effect of the shelving state is to reduce the success rate for entanglement generation and measurement by of order a few percent. Finally, we should note that the effect of the shelving state on the nuclear spin state is currently not known, and could potentially complicate the sequence of operations necessary upon detection of a shelving event.

[1] N. Gisin, G. Riborty, W. Tittel, and H. Zbinden, Rev. Mod. Phys **74**, 145 (2002).
[2] G. Brassard, N. Lutkenhaus, T. More, and B. Sanders, Phys. Rev. Lett. **85**, 1330 (2000).
[3] H. J. Briegel, W. Dur, J. I. Cirac, and P. Zoller, Phys. Rev. Lett. **81**, 5932 (1998).
[4] M. Zukowski *et al.*, Phys. Rev. Lett. **71**, 4287 (1993).
[5] C. Bennett *et al*, Phys. Rev. Lett. **70**, 1895 (1993).
[6] D. Bouwmeester *et al.*, Nature **390**, 575 (1997).
[7] A. Ekert, Phys. Rev. Lett. **67**, 661 (1991).
[8] C. Bennett *et al.*, Phys. Rev. Lett. **76**, 722 (1996).
[9] D. Deutsch *et al.*, Phys. Rev. Lett. **77**, 2818 (1996).
[10] S. J. van Enk, J. I. Cirac, and P. Zoller, Science **279**, 205 (1998).
[11] L. Duan and H. Kimble, Phys. Rev. Lett. **92**, 127902 (2004).
[12] B. Blinov *et al.*, Nature **428**, 153 (2004).
[13] S. Bose *et al.*, Phys. Rev. Lett. **83**, 5158 (1999).
[14] J. Ye, D. W. Vernooy, and H. J. Kimble, Phys. Rev. Lett. **83**, 4987 (1999).
[15] L. M. Duan, M. D. Lukin, J. I. Cirac, and P. Zoller, Nature **414**, 413 (2001).
[16] L. I. Childress, J. M. Taylor, A. Sørensen, and M. Lukin, submitted to PRL, quant-ph/0410123 (2004).
[17] J. McKeever *et al.*, Science **303**, 1992 (2004).
[18] C. Kurtsiefer, S. Mayer, P. Zarda, and H. Weinfurter, Phys. Rev. Lett. **85**, 290 (2000).
[19] A. Beveratos *et al.*, Phys. Rev. Lett. **89**, 187901 (2002).
[20] P. Michler *et al.*, Science **290**, 2282 (2000).
[21] C. Santori *et al.*, Nature **419**, 594 (2002).
[22] C. Cabrillo, J. Cirac, P. Garcia-Fernandez, and P. Zoller, Phys. Rev. A **59**, 1025 (1999).
[23] D. Browne, M. Plenio, and S. Huelga, Phys. Rev. Lett. **91**, 067901 (2003).
[24] A. P. Nizovtzev *et al.*, Optics and Spectroscopy **94**, 848 (2003).
[25] A. Muller *et al.*, Appl. Phys. Lett. **70**, 793 (1997).
[26] C. Simon and W. Irvine, Phys. Rev. Lett. **91**, 110405 (2003).
[27] A. Sørensen and K. Mølmer, Phys. Rev. A **58**, 2745 (1998).
[28] S. van Enk, J. Cirac, and P. Zoller, Phys. Rev. Lett. **78**, 4293 (1997).
[29] K. Mølmer, Y. Castin, and J. Dalibard, J. Opt. Soc. Am. B **10**, 524 (1993).
[30] A. Sørensen and K. Mølmer, Phys. Rev. Lett. **90**, 127903 (2003).
[31] S. Barrett and P. Kok (2004), quant-ph/0408040.
[32] F. Jelezko *et al.*, Phys. Rev. Lett. **92**, 076401 (2004).
[33] F. Jelezko *et al.*, Phys. Rev. Lett. **93**, 130501 (2004).
[34] W. Dur, H. J. Briegel, J. I. Cirac, and P. Zoller, Phys. Rev. A. **59**, 169 (1999).
[35] W. Dur, Masters Thesis (1998).
[36] T. Gaebel *et al.*, New Journal of Physics **6**, 98 (2004).
[37] S. Kilin, private communication.
[38] T. Kennedy *et al.*, Appl. Phys. Lett. **83**, 4190 (2003).
[39] A. Imamoglu *et al.*, Phys. Rev. Lett. **83**, 4204 (1999).
[40] E. Pazy, E. Biolatti, T. Calarco, I. D'Amico, P. Zanardi, F. Rossi, and P. Zoller, Europhys. Lett. **62**, 175 (2003), cond-mat/0109337.
[41] A. S. Bracker *et al.*, e-print:cond-mat/0408466 (2004).
[42] V. Golovach, A. Khaetskii, and D. Loss, eprint: cond-mat/0310655 (2003).
[43] C. Ramanathan *et al*, eprint: quant-ph/0408166 (2004).
[44] J. M. Taylor, C. M. Marcus, and M. D. Lukin, Phys. Rev. Lett. **90**, 206803 (2003).
[45] J. M. Taylor *et al.*, e-print: cond-mat/0407640 (2004).
[46] A. Kiraz *et al.*, Phys. Rev. B **65**, 161303(R) (2002).
[47] J. M. Taylor, A. Imamoglu, and M. Lukin, Phys. Rev. Lett. **91**, 246802 (2003).
[48] A. Imamoglu *et al.*, Phys. Rev. Lett. **91**, 017402 (2003).
[49] Raman transitions have been observed in a strong magnetic field by using the hyperfine interaction to mix the $|0\rangle$ and $|1\rangle$ states, but since such mixing involves the nuclear degree of freedom it is not applicable in the present context.
[50] For our entanglement generation scheme, such a filter will allow the desired narrow band of coherent light to pass through while rejecting the broad incoherent background. Consequently the filter will not decrease collection efficiency in the desired mode.